

In-silico evaluation of potential phytochemical targeting Glycoprotein-Gc of Hantavirus

Alisha Naz, Rabiya Maham, Eman Naeem, Muhammad Irfan Fareed, Muhammad Aourangzaib, Rana Muhammad Mateen*

Department of Life Sciences, School of Sciences, University of Management and Technology (UMT), Lahore, Punjab, Pakistan

ARTICLE INFO

Article Type:
Original Article

Keywords:
In-silico,
Hantavirus
spike glycoprotein
Antiviral
Zoonotic
RNA virus

**Corresponding author:*
Rana Muhammad Mateen
mateenibb@yahoo.com

Received on: Feb 28, 2024

Revised on: March 22, 2024

Accepted on: March 23, 2024

ABSTRACT

Background: Hantaviruses are novel zoonotic pathogens, which belong to the family *Hantaviridae*. The pathogens are tri-segmented, monopartite, enveloped, single-stranded (negative-sense) RNA viruses distributed worldwide, especially in Asia, Europe, and North and South America. It is asymptomatic and persistent in rodent host reservoirs. In rodents, the viruses do not cause infection but are transferred to humans by contaminated aerosolization of rodent excrement. Hantaan Orthohantavirus (HTNV) results in hemorrhagic fever with renal syndrome (HFRS) with an incredibly high mortality ratio. No drug is approved against it; therefore, this virus is classified as a Biosafety level 4 agent.

Objective: In this study, the surface spike (glycoprotein: Gc) of the virus genome is selected as an antiviral target, encoded by the M segments.

Methods: According to ADMET criteria, BBB- ligands were filtered out of 17967 compounds (phytochemicals). After careful analysis, the potential inhibitor against surface spike glycoprotein (Gc) was identified by using *in-silico* methodologies such as molecular docking, molecular dynamic (MD) simulations, and density functional theory (DFT).

Results: Verification of the selected structure of targeted protein molecule Gc was done using online servers. The protein–ligand complex shows deviation throughout the trajectory and the highest deviation which can be observed is more than 6Å. The root mean square deviation (RMSD) for ligand is stable and it does not deviate more than 2Å throughout 200ns. During the trajectory, hydrogen bonds were formed. It has been observed from the graph that the hydrogen bonds are forming but not uniform at some points.

Conclusion: In our current analysis, (2S,3R,4S,5S,6R)-2-[[[(6aR,11aR)-9-methoxy-6a,11a-dihydro-6H-[1] benzofuro[3,2-c]chromen-3-yl]oxy]-6-(hydroxymethyl)oxane-3,4,5-triol was identified as an effective compound for the therapeutic measures against Hantavirus. The outcomes of this study will contribute to a better understanding of Hantavirus-related diseases.

Introduction

Hantaviruses were first recognized during the pandemic in Korea near the Hantaan River among UN troops¹. Based on pathogenesis and geography, these are categorized into two distinct groups: Old World Hantaviruses which

comprise Puumala virus (PUUV), Hantaan Orthohantavirus (HTNV), Dobrava-Belgrade virus (DOBV), and Seoul Orthohantavirus (SEOV) species cause hemorrhagic fever with renal syndrome with a death rate of about (1% to 15%). New World Hantaviruses that involve

Sin Nombre virus (SNV), and Andes virus (ANDV) species cause (HCPS) Hantavirus cardiopulmonary syndrome with a mortality rate of about 40%². HFRS is characterized via vascular hemorrhage, hematuria, acute renal failure, and proteinuria. Due to its elevated death rate, it constitutes a significant risk to public health. In Asia and Europe, the most prevalent viruses responsible for HFRS include Puumala, Hantaan, Dobrava, and Seoul species³.

There are over 40 known species of Hantaviruses, of which 22 have been reported to be harmful to humans, and all of which use rodents as reservoirs. Hantaviruses infect rodents persistently without causing any symptoms, and the virus may persist in the animals for months or perhaps a lifetime⁴. They are asymptomatic due to complicated coevolution with various host species, they have developed distinctive ways of evading the innate immune system⁵. Hantavirus can enter the body by the bites of infected rodents, contaminated food, or by direct contact with eyes, mouth, or nose following exposure to excreta of rodents. Hantavirus is expected to cause the next health emergency conditions in upcoming years⁶. At present, there are no approved FDA antiviral medications or vaccinations to treat Hantavirus infections⁴. The Hantaviridae is a diverse and significant virus family of humans, plant pathogens, and animals that include five different genera: Orthobunyavirus, Phlebovirus, Tospovirus, and Nairovirus. The genus Hantavirus is a zoonotic, rodent-borne pathogen that causes severe hemorrhagic fever with renal syndrome⁷. Among the order *Bunyvirales*, there are 12 families of negative-sense RNA viruses, of which Hantaviridae is one⁸.

The Hantavirus genome consists of three segments M, L, and S, or tripartite, genome. All three segments have a specific role in the formation of Hantavirus. M segment of Hantavirus has a role in the formation of Glycoprotein Gn and Gc. L segment of Hantavirus has a role in the formation of RNA-dependent RNA polymerase. The last segment S plays a role in forming Non-structural proteins and nucleoproteins⁹. Hantavirus cells get entry into the host cell by the process of

endocytosis which is mediated by Clathrin protein which is present on the surface of the cell¹⁰. Receptors integrin beta 3 for the Hantavirus are present on endothelial cells and macrophages which are attached to the Gn and Gc (Glyco-proteins) of the Hantavirus and mediate the entry of Hantavirus into the cell¹¹. After getting entry into the host cell, the Hantavirus uncoated its genome. Through replication and transcription, viral RNA and viral proteins are made¹².

As, there are no approved FDA antiviral medications or vaccinations to treat Hantavirus infections⁴. Therefore, research is necessary to stop or inhibit the entry of hantavirus. In this study, the glycoprotein Gc, surface protein is targeted to restrict the entry of Hantavirus to human cell receptors with the help of *in-silico* analysis.

Research Approach and Strategies: The comprehensive methodology employed in the present analysis is provided in the figure 1.

D-Structure Selection of Target Protein: The first step was the selection of a 3D structure. The post-fusion conformation Gc 3D-structure is accessible on the Protein Data Bank (PDB). The crystal structure of Glycoproteins Gc (PDB: 5LJZ, resolution: 1.6Å) was selected and shown in the figure 2 from reacquired from the RCSB-PDB. Two parameters experimental resolution and method (X-Ray Diffraction) were seen for their structure's selection.

D-Structures Verification: The verification of this 3D structure was done by using these online software: PROCHECK¹³, Verify 3D¹⁴, as well as ERRAT¹⁵. From results, it has been concluded that this structure is acceptable for further processing. The results are given in the **table 2** below.

Active site prediction: Two software including CASTp: computed atlas of surface topography of proteins¹⁶ and PrankWeb: ligand binding site prediction¹⁷ were selected for the prediction of active residues at catalytic sites of protein Gc. All residues coming in pocket one of both CASTp and PrankWeb were chosen shown below in **Table 3**, that were further filtered to have common ones.

Studies on Molecular docking

Target protein preparation: The proteins were prepared for the molecular docking. Discovery Studio¹⁸ was used for clearing the protein chains and further charges were added using AutoDock Tools. In the discovery studio visualizer, the proteins were prepared in such a way that all the attached ligands were removed, including, heteroatoms, and water molecules.

Hydrogen atoms and Kollman charges were added using MGL tools¹⁹.

Grid Preparation: The docking step involves the preparation of a grid using the Autodock tool in which the active site amino acids present in suitable pockets are selected and a grid box is created with specific dimensions enlisted in Table 1

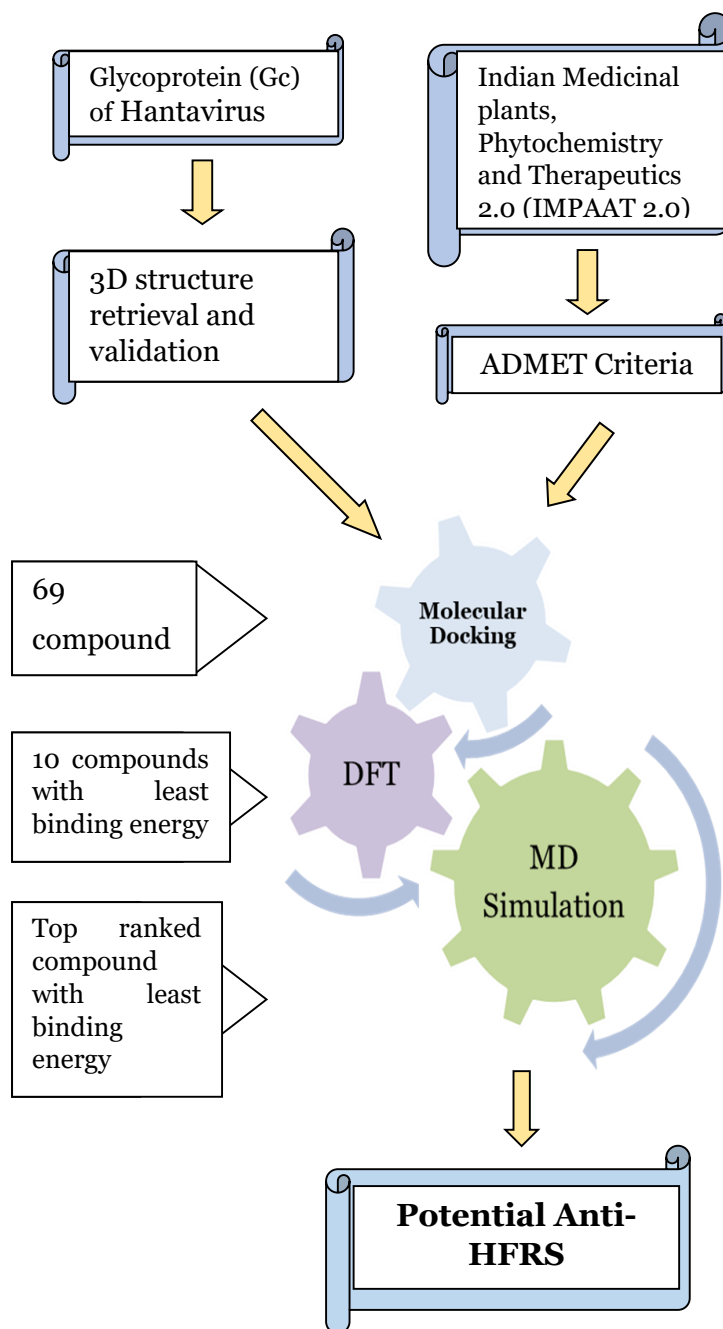


Figure 1: Overview of methodology

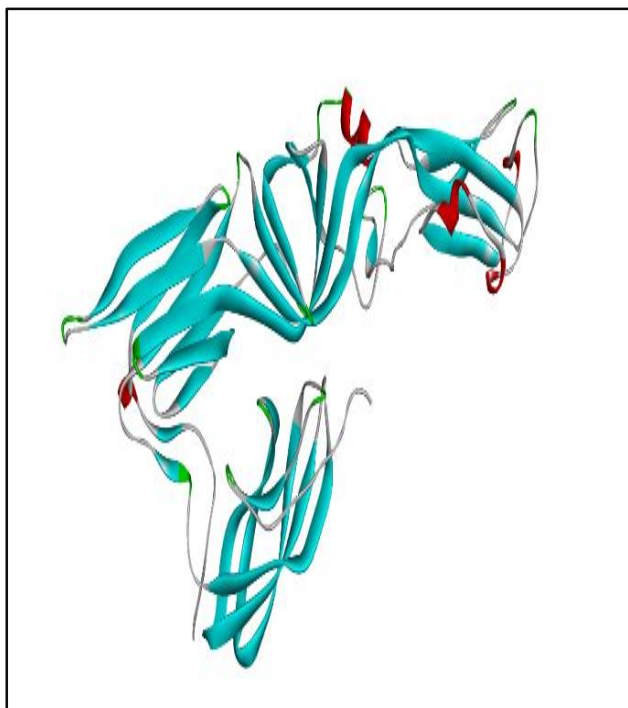


Figure 2: 3D-structure of Gc (PDB: 5LJZ, resolution: 1.6Å)

Table 1: Grid dimension for receptor protein preparation

Grid dimension for receptor protein preparation		
Coordinates	Center (Å)	Box size (points)
x	-15.070	24
y	-0.235	36
z	-9.507	52

Ligands Library Selection: For in silico analysis, the IMPPAT (Indian Medicinal Plants, Photochemistry and Therapeutics) library was used which contains 17967 compounds for docking purposes from online websites having a curated database²⁰.

Pharmacokinetics parameters and ligands library screening

The chosen IMPAAT library contains 17967 compounds which are distributed based on ADMET parameters. This parameter includes adsorption, distribution, metabolism, excretion as well as toxicity. The compounds are selected on the basis of the Lipinski Rule of Five (ROF). The rule of five includes parameters such as molecular weight < 500, H-bond acceptor < 10, Log P < 5, and H-bond donor < 5. The hERG - human ether-a-go-go-related gene encodes a protein that plays an essential role in the repolarization of cardiac. Inhibition of the

hERG K⁺ ion channel results in drug-induced QT syndrome²¹. Madin-Darby Canine Kidney (MDCK) cells are the property that helps us to predict the permeability of the compound through the biological barriers, especially intestinal barriers, and Blood Brain Barrier (BBB)²². Water solubility is another parameter with a recommended range ≥ 0.010 mg/mL, Log BB < -1, BCRP inhibition filter was also applied to sort out the further compounds present in the library. At last, the parameter of skin sensitivity (sensitizer) was applied.

Ligand Preparation: Discovery Studio visualizer¹⁸ as well as the Autodock tool was used for ligand preparation. During the preparation procedure, the first step was to convert all SDF files into PDB files by using Discovery Studio. Then the pdb files were opened in the Autodock tool¹⁹. Polar hydrogen, as well as Gasteiger charges, were done. After the addition, the PDBQT format of the files were saved.

Molecular docking: Auto Dock Vina v1.5.7²³ was used to dock ligands and targeted proteins. The top ten ordered ligands were selected on the basis of binding energy. These top-ranked compounds were visualized by means of the BIOVIA Discovery Studio Visualizer¹⁸. During visualization, the hydrophobic, electrostatic, and hydrogen bonding were examined. The compounds with the least binding energy in Docked results were subsequently chosen for further analysis.

Reference compound: A reference molecule is essential for the validation of docked results. At present, there are no approved FDA antiviral medications or vaccinations to treat Hantavirus infections⁴. For the prevention of Hantavirus, Chloroquine is considered effective²⁴, it is an anti-malarial drug, and therefore, Chloroquine was selected as a reference compound in this analysis. Chloroquine 3D structure was retrieved from Pubchem (CID: 2719). The active site residues of targeted protein Gc were selected to dock with the reference compound. A grid box was created and 2D and 3D bond interactions were visualized using BIOVIA Discovery Studio Visualizer¹⁸.

Density Functional Theory (DFT)

Density Functional Theory involves the computational quantum mechanical approach

to analyze the ligand's reactivity and its efficacy in interacting with target proteins ²⁵. An analysis using DFT was conducted to assess the reactivity of compounds exhibiting the least energy (BE) with the target Gc Glycoprotein amongst the top 10 ranked compounds. Chemical descriptors including (HOMO and LUMO) were examined in this analysis. The energy difference between the lowest unoccupied molecular orbital (LUMO) and the highest occupied molecular orbital (HOMO) of each compound was calculated using $E_{LUMO} - E_{HOMO}$. For the analysis of DFT, Gaussian 09 ²⁶ was used. The results were viewed by Gauss View 6.0 ²⁷. In the Method interface, the conditions such as ground-state, B3LYP, DFT, and Basis set: 6-31G were selected ²⁸. chk. file was selected to view the results.

Molecular Dynamic Simulation: Molecular dynamics simulation of the molecules showing the least binding energy (BE) in docking was done using Nano Scale Molecular Dynamics (NAMD). The variables and potential functions of the CHARM++ force field were utilized ²⁹.

Post simulation analysis: Visual Molecular Dynamics (VMD) v1.9.3 ³⁰ was utilized to study the dynamic properties of targeted proteins, stability of residual interaction as well as protein-ligand complexes. The properties including Root mean square deviation (RMSD), the root mean square fluctuation (RMSF) the total number of hydrogen bonds, protein-ligand complexes, and individual targeted proteins were determined using this tool.

Results

D-Structures Verification: Verification of the selected structure of targeted protein molecule Gc was done using online servers.

PROCHECK ¹³, Verify 3D ¹⁴, and ERRAT ¹⁵. The overall quality factor is good. There are a maximum number of residues in the allowed region according to the Ramachandran Plot, therefore, the protein is considered stable for further analysis. The data on stability is summarized in the table 2 below.

Suitable pocket Amino acids: The common amino acids filtered from both software Castp and Prankweb are listed here

Table 2: Target protein stability data

Online server utilized	Gc (Glycoprotein of HTNV)
ERRAT	The overall quality factor: 93.04
Verify 3D	Pass
Ramachandran Plot (PROCHECK)	Residues in allowed region: 99.7%

Table 3: List of common amino acids filtered from the most suitable pocket of both software.

Software	Most suitable pockets
Common Amino acids from CASTp, Prank-Web	Asp_11, Asn_12, His_14, Arg_152, Lys_168, Ile_169, Ile_170, Asp171, Asp_174, Cys_175, Ser_358, Lys_360, Cys_367, His_399, Gly_400, Glu_401

Screened ligands based on ADMET Criteria:

The phytochemical compounds were screened on the basis of ADMET criteria. These include the properties related to Absorption, Distribution, metabolism, excretion, and toxicity. The optimum values of the criteria are listed in the table 4 below. Out of total 17967 compounds, only 69 were selected. BBB-compounds were selected that could not enter or pass the blood-brain barrier. For further analysis, these screened compounds were selected.

Molecular Docking: A total of 17967 compounds, 69 were docked with Glycoprotein Gc of HNTV utilized as receptors. Based on the lowest binding energies, the docked compounds were ranked. The top docked compounds with target protein Gc with their IUPAC names, structures, molecular formula, and type of interactions as well as residual interactions of target protein Gc are listed in Table 5

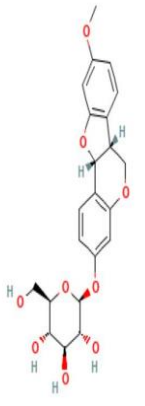
Table 4: Compounds fulfilling the ADMET analysis

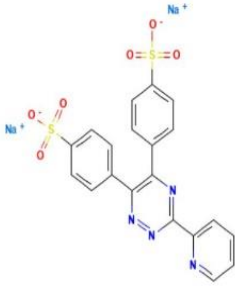
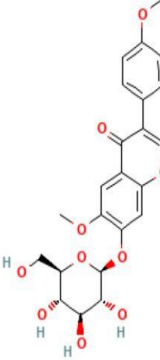
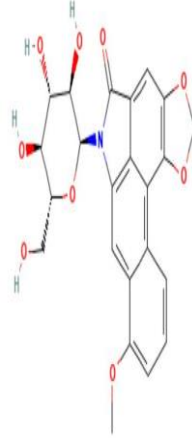
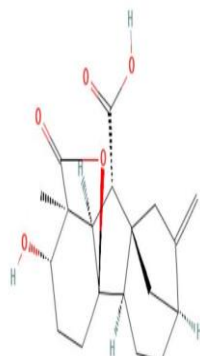
Sr No.	ADMET Attributes	Recommended Thresholds	Screened Ligands
1.	Lipinski's rule of five (ROF) Hydrogen bond acceptor Molecular Weight Hydrogen bond donor Log P	≤ 5 <500 Dalton ≤ 10 ≤ 5	17967
2.	Water solubility (Sw)	≥ 0.010 mg/mL	4899
3.	Apparent Madin-Darby canine kidney cell permeability (MDCK)	≥ 30 cm/s $\times 10^7$	4078
4.	Log BB	< -1 (for BBB-)	165
5.	Blood Brain Barrier filter	Low (%) (for BBB-)	112
6.	BCRP_Inh	No	102
7.	hERG Filter	No	100
8.	hERG pIC50	< 5.5	88
9.	Skin sensitivity (sensitizer)	No	69

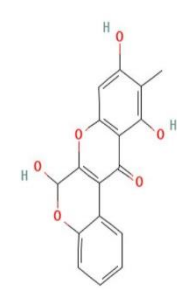
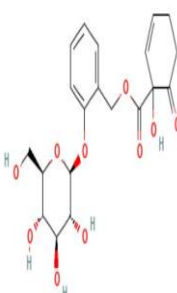
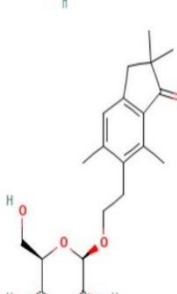
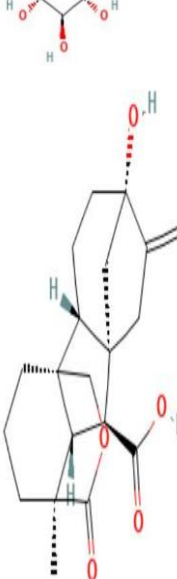
Number of compounds fulfilling ADMET criteria = 69

Table 5: PubChem ID, IUPAC name, Binding energies, 2D structures, MF, and interacting amino acids with Glycoprotein Gc

PubChem ID, Binding Energies, Residual Interactions, Molecular Formula, Structure Of Top Ranked Compounds Of Docking With Gc

Sr#	Pubchem ID	IUPAC Name	BE (kcal/mol)	Structure	Molecular formula	Residual interaction
1	23724664	(2S,3R,4S,5S,6R)-2-[[[(6aR,11aR)-9-methoxy-6a,11a-dihydro-6H-[1]benzofuro[3,2-c]chromen-3-yl]oxy]-6-(hydroxymethyl)oxane-3,4,5-triol	-9.3		C ₂₂ H ₂₄ O ₉	HB: Arg152, Asp171, Arg290, Glu292 HP: Cys367, Ala370, Lys360, Ala370 Electrostatic: Arg152, Lys360, Asp171 Others: Cys367

2	34127	disodium;4-[3-pyridin-2-yl-6-(4-sulfonatophenyl)-1,2,4-triazin-5-yl]benzenesulfonate	-8.8		$C_{20}H_{12}N_4Na_2O_6S_2$	HB: Arg152, Met172, Ile169, Asn12 HP: His14, His399 Electrostatic: His14, Arg152, Lys360, Asp171, Asp174 Others: Cys367
3	10095770	6-methoxy-3-(4-methoxyphenyl)-7-[(2S,3R,4S,5S,6R)-3,4,5-trihydroxy-6-(hydroxymethyl)oxan-2-yl]oxychromen-4-one	-8.8		$C_{23}H_{24}O_{10}$	HB: Arg152, Arg290, Lys360 HP: Lys360, Cys367, Ile169, Ile366 Electrostatic: Asp171
4	159819	14-methoxy-10-[(2S,3R,4S,5S,6R)-3,4,5-trihydroxy-6-(hydroxymethyl)oxan-2-yl]-3,5-dioxo-10-azapentacyclo[9.7.1.0 ^{2,6} .0 ^{8,19} .0 ^{13,18}]nonadecan-1(18),2(6),7,11(19),12,14,16-heptaen-9-one	-8.7		$C_{23}H_{21}NO_9$	HB: Arg152, Glu401, Ile169, Lys364, Ser154 HP: Ile169, Ala365, Ile366 Electrostatic: Arg290, Glu292
5	3034393	(1R,2R,5S,8R,9S,10R,11S,12S)-12-hydroxy-11-methyl-6-methylidene-16-oxo-15-oxapentacyclo[9.3.2.1 ^{5,8} .0 ^{1,10} .0 ^{2,8}]heptadecane-9-carboxylic acid	-8.6		$C_{19}H_{24}O_5$	HB: Val189, Ile151, Arg152

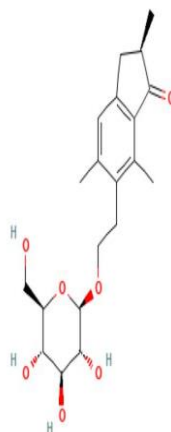
6	14018348	6,9,11-trihydroxy-10-methyl-6H-chromeno[3,4-b]chromen-12-one	-8.6		C ₁₇ H ₁₂ O ₆	HB: Trp214, Thr216, Asp226, Leu236 HP: Thr216, Leu236, Cys219, Leu71, Lys147 Others: Cys219
7	115158	[2-[(2S,3R,4S,5S,6R)-3,4,5-trihydroxy-6-(hydroxymethyl)oxan-2-yl]oxyphenyl]methyl 1-hydroxy-6-oxocyclohex-2-ene-1-carboxylate	-8.4		C ₂₀ H ₂₄ O ₁₀	HB: Arg290, Lys294, Arg152 HP: Ile169, Lys294, Arg156
8	169737	2,2,5,7-tetramethyl-6-[2-[(2R,3R,4S,5S,6R)-3,4,5-trihydroxy-6-(hydroxymethyl)oxan-2-yl]oxyethyl]-3H-inden-1-one	-8.4		C ₂₁ H ₃₀ O ₇	HB: Arg152, Asp171, Ala365, Asp171, Ser154 HP: Ile169, Ile366 Electrostatic: Arg290, Glu292
9	443756	(1R,2R,5S,8S,9S,10S,11S)-5-hydroxy-11-methyl-6-methylidene-12-oxo-13-oxapentacyclo[9.3.3.1 ^{5,8} .0 ^{1,10} .0 ^{2,8}]octadecane-9-carboxylic acid	-8.4		C ₂₀ H ₂₆ O ₅	HB: Asn173, Met172 HP: Ile151, Met172

10

134279

(2R)-2,5,7-trimethyl-6-[2-[(2R,3R,4S,5S,6R)-3,4,5-trihydroxy-6-(hydroxymethyl)oxan-2-yl]oxyethyl]-2,3-dihydroinden-1-one

-8.3

C₂₀H₂₈O₇

HB: Arg152,
Lys360, Ala365,
Ser154
HP: Ile169
Electrostatic:
Arg290, Glu292

Out of 10 of top-ranked compounds, the compound with the least binding energy was selected for further analysis. Gc with ((2S,3R,4S,5S,6R)-2-[[[(6aR,11aR)-9-methoxy-6a,11a-dihydro-6H-[1]benzofuro[3,2-c]chromen-3-yl]oxy]-6-(hydroxymethyl)oxane-3,4,5-triol) was analyzed. BIOVIA Discover Studio was utilized for the visualization of interactions. The best binding pose of ligand (CID: 23724664) with Gc protein is shown below in

Figure 3:

Glycoprotein Gc protein with ligand (CID: 23724664)

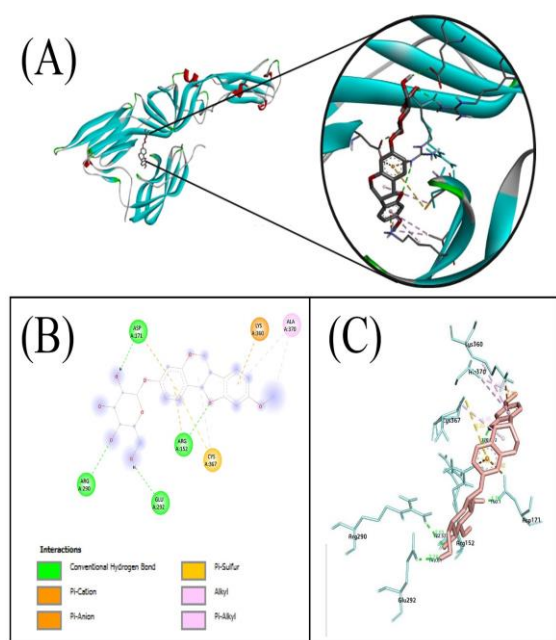


Figure 3: Best binding conformation.

Best binding conformation of ligand in the active site pocket of Gc (A) Binding pose of molecule (2S,3R,4S,5S,6R)-2-[[[(6aR,11aR)-9-methoxy-

6a,11a-dihydro-6H-[1]benzofuro[3,2-c]chromen-3-yl]oxy]-6-(hydroxymethyl)oxane-3,4,5-triol with protein 5LJZ. (B) 2D representation (C) Interaction diagram of Gc with (2S,3R,4S,5S,6R)-2-[[[(6aR,11aR)-9-methoxy-6a,11a-dihydro-6H-[1]benzofuro[3,2-c]chromen-3-yl]oxy]-6-(hydroxymethyl)oxane-3,4,5-triol

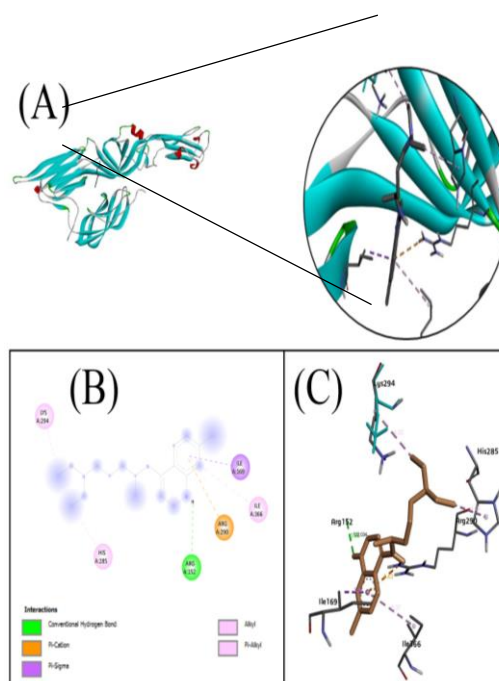


Figure 4: Best binding of reference ligand

Best binding poses of reference ligand in the binding cavity of Gc. (A) shows the best conformation of binding of reference molecule with Gc (B) shows the 2D diagram of bonding (C) shows the interactions of reference compound with the active site amino acids

Docking Results of Reference Compound: Chloroquine was selected as the control ligand.

Chloroquine was docked to the active residue of Gc. The complex Gc-chloroquine is shown in Figure 4. Chloroquine shows a BE of -6.7kcal/mol Gc. The Hydrogen bonding, and other interactions as well as bond length, and bond angles are shown in Figure 4

Analysis using Density Functional Theory (DFT): The gap between E_{LUMO} and E_{HOMO} was used to calculate the reactivity of selected compounds. A compound with a large energy gap would have a high kinetic stability and minimal chemical reactivity, and vice versa. The relatively small energy gap exhibited that the compound has low kinetic stability as well as favorable chemical reactivity towards the

respective Glycoprotein Gc. In a low energy gap, it is favorable energetically to add particles (electron) to a high-located LUMO orbital and remove particles (electrons) from a low-located HOMO orbital ³¹. The DFT analysis of compound (2S,3R,4S,5S,6R)-2-[[[(6aR,11aR)-9-methoxy-6a,11a-dihydro-6H-[1]benzofuro[3,2-c]chromen-3-yl]oxy]-6-(hydroxymethyl)oxane-3,4,5-triol. The HOMO value is 0.20620-eV and LUMO orbital energies are 0.00935 -eV, respectively with an energy gap of 0.19685eV.

The pictorial representation is given below in the figure 5.

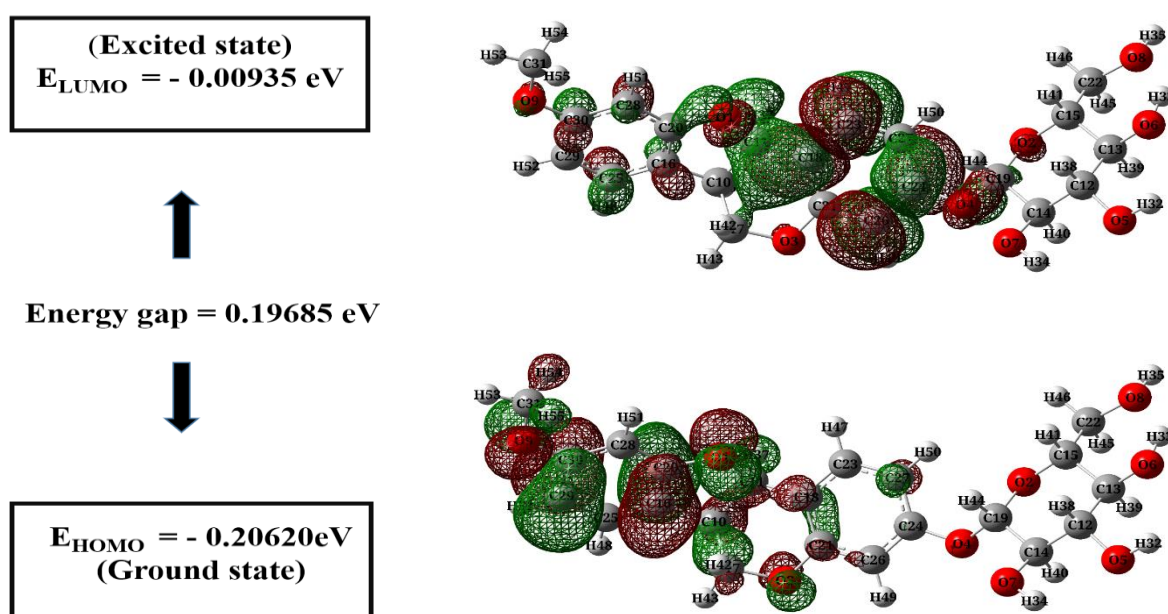


Figure 5: Selected ligand's (2S,3R,4S,5S,6R)-2-[[[(6aR,11aR)-9-methoxy-6a,11a-dihydro-6H-[1]benzofuro[3,2-c]chromen-3-yl]oxy]-6-(hydroxymethyl)oxane-3,4,5-triol. Quantum chemical descriptors. The HOMO and LUMO orbital energies are 0.20620-eV and 0.00935 -eV, respectively with an energy gap of 0.19685eV.

MD simulation examination: The study of MD simulation throughout the trajectory is given in Figure 6. The analysis was done for 200ns. The protein-ligand complex shows deviation throughout the trajectory and the highest deviation which can be observed is more than 6Å. The root mean square deviation (RMSD) for ligand is stable and it does not deviate more than 2Å throughout 200ns. During the trajectory, hydrogen bonds were formed. It has been observed from the graph that the hydrogen bonds are forming but not uniform at some

points. There are a total of 18 hydrogen bonds formed between the acceptor and the donor. The highest occupancy of a hydrogen bond is 69.79% between donor and acceptor residue (Asp171-side) which is an active site amino acid. The hydrogen bonding with their respective occupancy is shown in Table 6. Similarly, root mean square fluctuation (RMSF) helps in the determination of single residual fluctuation in the target protein. The RMSF in the first and last 1000 frames of the simulation trajectory was calculated. It has been

observed that the residues displayed balanced RMSF and it does not exceed more than 3 Å through trajectory except at the start where the highest value is about 4 Å.

Table 6: Number of hydrogen bonds throughout the trajectory

Donor	Acceptor	Occupancy
UNK1-Side	ASP171-Side	69.79%
UNK1-Side	GLU292-Side	27.79%
ARG290-Side	UNK1-Side	10.97%
UNK1-Side	ARG152-Main	3.64%
SER154-Side	UNK1-Side	2.55%
UNK1-Side	TYR153-Main	0.22%
UNK1-Side	ILE64-Main	0.03%
UNK1-Side	SER154-Side	0.68%
UNK1-Side	ALA365-Main	0.58%
UNK1-Side	ILE169-Main	0.49%
LYS360-Side	UNK1-Side	0.27%
ASP171-Main	UNK1-Side	0.02%
ARG152-Side	UNK1-Side	0.02%
LYS168-Side	UNK1-Side	0.02%
ALA370-Main	UNK1-Side	0.01%
CYS367-Main	UNK1-Side	4.19%
SER358-Side	UNK1-Side	0.02%
SER372-Side	UNK1-Side	0.01%

Discussion

At present, there are no approved FDA antiviral medications or vaccinations to treat Hantavirus infections⁴. Due to the high mortality rate, the emergence of the Hantavirus infection will likely cause the next few public health emergencies⁶. Therefore, research is necessary to stop or inhibit the entry of hantavirus. In this study, the glycoprotein Gc, surface protein is targeted to restrict the entry of Hantavirus to human cell receptors with the help of *in-silico* analysis.

Various studies on the discovery of potential inhibitors are going on. In this study, the strategy was used to find out a potential compound that could inhibit or prevent hantavirus infection. The 3D structure of the target was retrieved from PDB displaying effective resolution determined by X-ray

crystallography. The post-fusion conformation is also explained in³². The docking results showing the binding energies ranged from -9.3 to -8.3 kcal/mol. The evaluation of binding energies of both the selected compound and reference molecule confirms that the ligand **CID: 23724664** is a potential inhibitor against the hantavirus. The energy gap of HOMO and LUMO orbital energies is 0.19685eV. The lower energy gap as indicated by³³ the effective good reactivity ligand. Thus, our selected ligand 2S,3R,4S,5S,6R)-2-[[[(6aR,11aR)-9-methoxy-6a,11a-dihydro-6H-[1] benzofuro[3,2-c]chromen-3-yl]oxy]-6-(hydroxymethyl) oxane-3,4,5-triol is reactive towards the target protein Gc.

The stability was determined using MD simulation. The RMSD graph indicates some fluctuations but it goes stable at the end during the trajectory of 200ns. The RMSD of the ligand is below 2 Å throughout the trajectory indicating the stability of molecules as explained by³⁴. The RMSF values show fluctuation at some residues but the active sites amino acids are stable throughout the trajectory. The hydrogen bonds forming during the trajectory are uniform at some points indicating stability³⁵. The highest occupancy of a hydrogen bond is 69.79% between donor and acceptor residue (Asp171-side) which is an active site amino acid, therefore, this can be effective. This ligand can be a potential compound to block the entry of Hantavirus.

Conclusion

Virtual screening has emerged as a cornerstone in drug development methodologies. The streamlined computational processes involved in *in-silico* analysis significantly reduce the time and resources traditionally required for drug discovery. In our analysis, we submerised that the phytochemical 2S,3R,4S,5S,6R)-2-[[[(6aR,11aR)-9-methoxy-6a,11a-dihydro-6H-[1] benzofuro[3,2-c]chromen-3-yl]oxy]-6-(hydroxymethyl) oxane-3,4,5-triol can be the potential inhibitor for the hantavirus. The outcomes of this study encourage *in-vivo* examination.

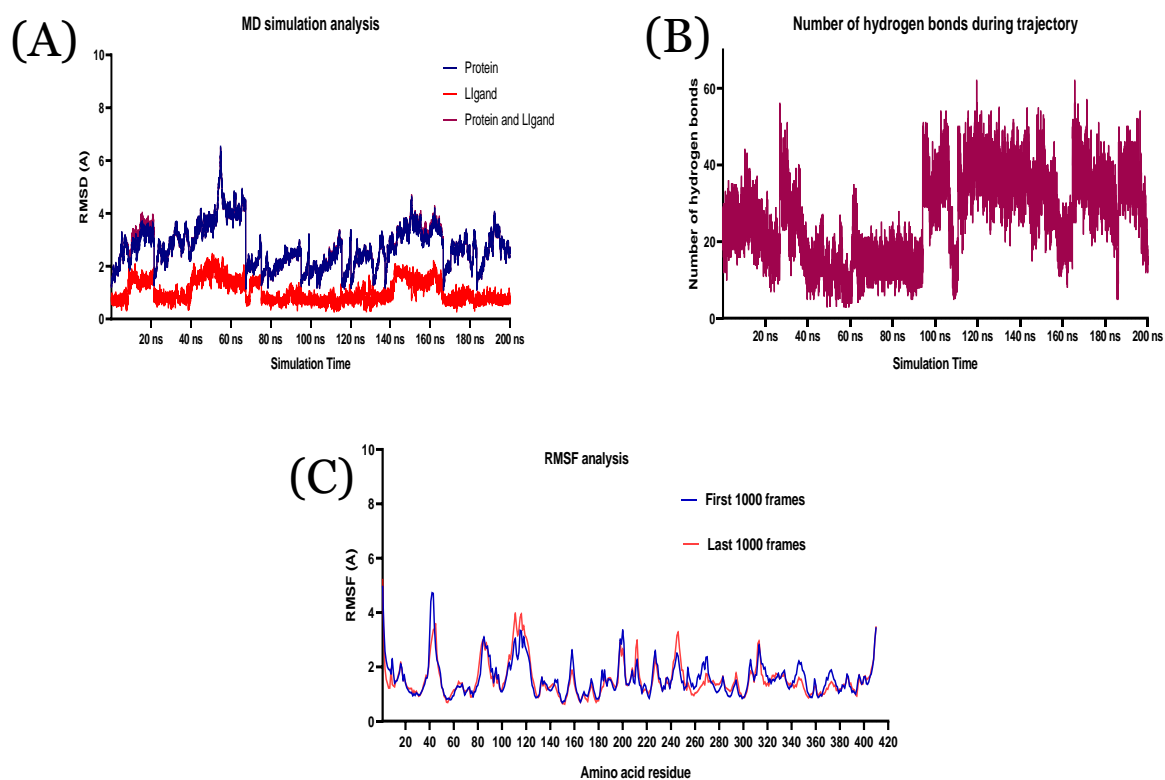


Figure 6: shows the RMSD value for ligand CID: 23724664 and protein 5LJZ, and the highest deviation is 6 Å (B) Showing that hydrogen bonding formed during 200ns (C) The RMSF analysis of complex during the 200ns run.

Conflict of Interest: The authors have no competing interests.

Funding Source: No funding was received from any agency for this study

References

- McCormick J, Palmer E, Sasso D, Kiley M. Morphological identification of the agent of Korean hemorrhagic fever (hantaan virus) as a member of the bunyaviridae. *The Lancet*. 1982;319(8275):765-8.
- Engdahl TB, Crowe Jr JE. Humoral immunity to hantavirus infection. *MSphere*. 2020;5(4):10.1128/msphere.00482-20.
- Faisal S, Badshah SL, Sharaf M, Abdalla M. Insight into the hantaan virus rna-dependent rna polymerase inhibition using in-silico approaches. *Molecular Diversity*. 2022;1-18.
- Munir N, Jahangeer M, Hussain S, Mahmood Z, Ashiq M, Ehsan F, et al. Hantavirus diseases pathophysiology, their diagnostic strategies and therapeutic approaches: A review. *Clinical and Experimental Pharmacology and Physiology*. 2021;48(1):20-34.
- Tariq M, Kim D-M. Hemorrhagic fever with renal syndrome: Literature review, epidemiology, clinical picture and pathogenesis. *Infection & chemotherapy*. 2022;54(1):1.
- Singh S, Numan A, Sharma D, Shukla R, Alexander A, Jain GK, et al. Epidemiology, virology and clinical aspects of hantavirus infections: An overview. *International Journal of Environmental Health Research*. 2022;32(8):1815-26.
- Willensky S, Bar-Rogovsky H, Bignon EA, Tischler ND, Modis Y, Dessau M. Crystal structure of glycoprotein c from a hantavirus in the post-fusion conformation. *PLoS Pathogens*. 2016;12(10):e1005948.
- Serris A, Stass R, Bignon EA, Muena NA, Manuguerra J-C, Jangra RK, et al. The hantavirus surface glycoprotein lattice and its fusion control mechanism. *Cell*. 2020;183(2):442-56. e16.
- Olal D, Daumke OJCR. Structure of the hantavirus nucleoprotein provides insights into the mechanism of rna encapsidation. 2016;14(9):2092-9.

10. Faisal S, Badshah SL, Sharaf M, Abdalla MJMD. Insight into the hantaan virus rna-dependent rna polymerase inhibition using in-silico approaches. 2022;1-18.
11. Singh S, Numan A, Sharma D, Shukla R, Alexander A, Jain GK, et al. Epidemiology, virology and clinical aspects of hantavirus infections: An overview. 2022;32(8):1815-26.
12. Kanerva M, Mustonen J, Vaehri AJRimv. Pathogenesis of puumala and other hantavirus infections. 1998;8(2):67-86.
13. Laskowski RA, MacArthur MW, Moss DS, Thornton JM. Procheck: A program to check the stereochemical quality of protein structures. Journal of applied crystallography. 1993;26(2):283-91.
14. Eisenberg D, Lüthy R, Bowie JU. [20] verify3d: Assessment of protein models with three-dimensional profiles. Methods in enzymology. 277: Elsevier; 1997. p. 396-404.
15. Colovos C, Yeates TO. Verification of protein structures: Patterns of nonbonded atomic interactions. Protein science. 1993;2(9):1511-9.
16. Dundas J, Ouyang Z, Tseng J, Binkowski A, Turpaz Y, Liang J. Castp: Computed atlas of surface topography of proteins with structural and topographical mapping of functionally annotated residues. Nucleic acids research. 2006;34(suppl_2):W116-W8.
17. Jendele L, Krivak R, Skoda P, Novotny M, Hoksza D. Prankweb: A web server for ligand binding site prediction and visualization. Nucleic acids research. 2019;47(W1):W345-W9.
18. Biovia DS. Discovery studio visualizer v21. 1.0. 20298. San Diego: Dassault Systèmes. 2021.
19. Di Muzio E, Toti D, Polticelli F. Dockingapp: A user friendly interface for facilitated docking simulations with autodock vina. Journal of Computer-Aided Molecular Design. 2017;31:213-8.
20. Mohanraj K, Karthikeyan BS, Vivek-Ananth RP, Chand RPB, Aparna SR, Mangalapandi P, et al. Imppat: A curated database of indian medicinal plants, phytochemistry and therapeutics. Scientific reports. 2018;8(1):4329.
21. AlRawashdeh S, Chandrasekaran S, Barakat KH. Structural analysis of hERG channel blockers and the implications for drug design. Journal of Molecular Graphics and Modelling. 2023;120:108405.
22. Feng B, West M, Patel NC, Wager T, Hou X, Johnson J, et al. Validation of human mdr1-mdck and bcrp-mdck cell lines to improve the prediction of brain penetration. Journal of pharmaceutical sciences. 2019;108(7):2476-83.
23. Trott O, Olson AJ. Autodock vina: Improving the speed and accuracy of docking with a new scoring function, efficient optimization, and multithreading. Journal of computational chemistry. 2010;31(2):455-61.
24. Vergote V, Laenen L, Mols R, Augustijns P, Van Ranst M, Maes P. Chloroquine, an anti-malaria drug as effective prevention for hantavirus infections. Frontiers in Cellular and Infection Microbiology. 2021;11:580532.
25. Orio M, Pantazis DA, Neese F. Density functional theory. Photosynthesis research. 2009;102:443-53.
26. Frisch M, Trucks G, Schlegel H, Scuseria G, Robb M, Cheeseman J, et al. Gaussian 09 revision a. 02, 2009, gaussian inc. Wallingford CT. 2009;66:219.
27. Dennington R, Keith TA, Millam JM. Gaussview, version 6.0. 16. Semicem Inc Shawnee Mission KS. 2016.
28. Rauhut G, Pulay P. Transferable scaling factors for density functional derived vibrational force fields. The Journal of Physical Chemistry. 1995;99(10):3093-100.
29. Hollingsworth SA, Dror RO. Molecular dynamics simulation for all. Neuron. 2018;99(6):1129-43, Phillips JC, Braun R, Wang W, Gumbart J, Tajkhorshid E, Villa E, et al. Scalable molecular dynamics with namd. Journal of computational chemistry. 2005;26(16):1781-802.
30. Tariq A, Mateen RM, Afzal MS, Saleem M. Paromomycin: A potential dual targeted drug effectively inhibits both spike (s1) and main protease of covid-19. International Journal of Infectious Diseases. 2020;98:166-75.
31. Humphrey W, Dalke A, Schulten K. Vmd: Visual molecular dynamics. Journal of molecular graphics. 1996;14(1):33-8.
32. Naeem I, Mateen RM, Sibtul Hassan S, Tariq A, Parveen R, Saqib MAN, et al. In silico identification of potential drug-like molecules against glycoprotein of nipah virus by molecular docking, dft studies, and molecular dynamic simulation. Journal of Biomolecular Structure and Dynamics. 2023;41(15):7104-18.
33. Rissanen I, Stass R, Zeltina A, Li S, Hepojoki J, Harlos K, et al. Structural transitions of the conserved and metastable hantaviral glycoprotein envelope. Journal of virology. 2017;91(21):10-1128.

34. Bitew M, Desalegn T, Demissie TB, Belayneh A, Endale M, Eswaramoorthy R. Pharmacokinetics and drug-likeness of antidiabetic flavonoids: Molecular docking and dft study. Plos one. 2021;16(12):e0260853.
35. Singh DB, Pathak RK. Computational approaches in drug designing and their applications. Experimental protocols in biotechnology. 2020:95-117.
36. Yunta MJR. It is important to compute intramolecular hydrogen bonding in drug design. Am J Model Optim. 2017;5(1):24-57.